ISSN: 2515-8260, Volume 07, Issue 11, 2020

ELECTROCHEMICAL STUDIES OF (Ce / Mo / V) MIXED METAL OXIDE NANOCOMPOSITES FOR ENERGY STORAGE APPLICATION

B.Uthira selvi [a*], Jessica Fernando [b], C.Vedhi [b],

Manikanda Bharath. K[c],Sanjay Kumar. C[d]

[a*]*Research Scholar (19112232032001), PG & Research Department of Chemistry, V.O.Chidambaram College, Tuticorin-628008, Affiliated to ManonmaniamSundaranar University, Abishekapatti, Tirunelveli-627012, Tamilnadu, India*
[b] *Assistant Professor, PG and Research Department of Chemistry, V.O.Chidambaram College, Tuticorin-628008, Affiliated to ManonmaniamSundaranar University, Abishekapatti, Tirunelveli-627012, Tamilnadu, India*
[c]*Institute for Ocean Management, Anna University, Chennai - 600025, Tamilnadu, India,*
[d]*Indian Institute Of Technology, Delhi,*
author:uthiraselvi14@gmail.com

Abstract

The synthesis and electrochemical analysis of (Ce/Mo/V) mixed metal oxide nanocomposites are widely used for supercapacitor application. In this context, the nanocomposites were synthesized from their precursors and characterized using Ultraviolet visible spectroscopy, Fourier Transform Infrared spectroscopy (FTIR), Field emission scanning electron microscope (FESEM) and X-Ray diffraction analysis. The maximum absorption (Λ_{max})values were used to calculate the band gap energies of the composites. IR spectrum confirms the presence of all three metal-oxide stretching vibrationswith V–O stretching vibration at 616cm^{-1} and Ce–O stretching is seen at 469cm^{-1}. XRD shows the sharp peaks which may be due to crystalline nature of the composites and the size is ~44.66 nm. The FE-SEM images show the surface morphology as agglomerated grains and the particle size is in the nanometre range. Electrochemical impedance spectroscopy (EIS) measured double layer capacitance of 1.265x10^{-6}with the mixed metal oxide nanocomposites. The specific capacitance value is calculated to be 102 F/g for (Ce/Mo/V) mixed metal oxide nanocomposites and therefore can be a suitable electrode material for the fabrication of supercapacitor device.

Keywords: MMO, FE-SEM; Supercapacitor; nanocomposites; double layer capacitance; Specific capacitance.

1. INTRODUCTION

The electronic devices and electric vehicles which is used for energy storage devices. Electrochemical capacitors [1], also known as ultra-capacitors or supercapacitors have been widely used in many areas such as memory backup systems, military device, mobile electronic devices, aircraft and hybrid electric vehicles due to their wide operation temperature range, long cycling stability, improved safety and ultra-high power density [2-4]. However, they suffer from lower energy density, which limits their potential applications. As a result, improvement of the energy density of supercapacitors is essential to meet the future energy demands [5]. Supercapacitor or ultra-capacitor is the most optimistic electrode material for the next generation of energy storage device due to their distinctive properties of rapid charge–discharge behaviour[6]and higher specific power density than fuel cells and batteries while having higher energy densities than double layer capacitors[7].The commercially available supercapacitors have very low energy density (5–10 Wh/kg) which is considerably lower than the lithium-ion batteries (120–170 Wh/kg)[8]. Like lithium batteries,

supercapacitors are having the ability to store energy and it can also be recharged in a very short time. As a result, the supercapacitors have received great interest for the researchers on energy storage applications. They also focus on desired energy density while designing supercapacitors; it needs suitable electrode material with the following essential characteristics as high surface area, good electrochemical reversibility[9], high thermal and chemical stability, and high electronic conductivity. So far, research has spotlighted on electrode materials such as high surface area carbonaceous materials [9-11], conducting polymers [12-15], transition metal oxides (TMOs) [16, 17]and mixed composites as well [18, 19]. Transition metal oxides such as RuO_2, IrO_2, TiO_2, NiO, CeO_2, MoO_3 and MnO_2 have been studied as redox supercapacitor materials generated by fast redox reactions [20]. Among these oxides, RuO_2 has been extensively studied and has been found to be the most promising redox supercapacitor material[21], but its high cost, resource abundance and toxic nature limit its broad applications. CeO_2 is a comparatively new supercapacitor material for its wide-ranging use in applications like oxygen storage [22, 23], catalytic converters [24, 25], biosensors [26, 27] and solid oxide fuel cells [28, 29]. Binary metal oxides of cerium molybdate have received much attention for its high performance supercapacitive materials. Abdollah Yari etal., synthesized CeMO/NPRGO nanocomposite and reported the specific capacitance as 638 Fg^{-1}[30].S.Chandra Sekhar et al., prepared silver nanoparticles-decorated $Ce_6Mo_{10}O_{39}$ marigold flower-like structures and its electrochemical performance was achieved 62 $\mu Ah/cm^2$ at 2 mA/cm^2 [31]. CeO_2 nanoparticles and carbon coated CeO_2 nanorods synthesized by a simple hydrothermal process displays a specific capacitance of 381 Fg^{-1} and 400 Fg^{-1}respectively [32]. The metal oxide nanocomposites can enhance surface electrochemical reactivity and increase the capacity retention capability for a higher number of cycles. The high redox potential of these metal oxide nanocomposites is expected to provide a higher potential window as well as increase the specific capacity and energy density of the system. It involves the application of energy storage devices and in particular, electrochemical capacitors, have attracted tremendous attention for future energy storage applications. Such investigations have exposed that mixed metal oxides nanocomposites have higher capacitance values when compared to single oxides from literature. Besides the admirable features, the combination of cerium oxide with other metal oxide composites such as Vanadium oxide [33], Molybdenum oxide [34] and their combination is discussed. In the present study we used mixed metal oxide to characterize the nanocomposites using FE-SEM, FTIR and XRD. Furthermore, we analysed the sample and studied the electrochemical properties. The size of nanocomposites and crystallinity calculated using Scherrer's formula. The morphological changes of mixed metal oxides studied through FE-SEM. The calculation of specific capacitance in this study useful to identify the performance and energy storage of supercapacitors.

2. MATERIALS AND METHODS

2.1. Materials

Ammonium ceric nitrate ($(NH_4)_2Ce\ (NO_3)_6$) CAS number of 16774-21-3, Ammonium meta vanadate (NH_4VO_3) CAS number of 7803-55-6, Ammonium molybdate ($(NH_4)_6Mo_7O_{24}$) CAS number of 12054-85-2, Sodium docusate ($C_{20}H_{37}NaO_7S$) CAS number of 577-11-7and

sodium hydroxide were procured from Merck, India. Double distilled water was used in synthetic and analytical procedures. All chemicals were used as supplied without further purification.

2.2. Synthesis of (Ce/Mo/V) Mixed metal oxide nanocomposites

0.1 N 100mL solutions of Ammonium ceric nitrate $(NH_4)_2Ce(NO_3)_6$, Ammonium meta vanadate (NH_4VO_3) and Ammonium molybdate ($(NH_4)_6Mo_7O_{24}$) were prepared by dissolving the salts separately in deionised water under constant stirring for 15 min. The three solutions were mixed together, and a saturated solution of sodium docusate $C_{20}H_{37}NaO_7S$ surfactant was added drop wise to the mixture. Finally, NaOH was added until the complete gel was formed. This solution was magnetically stirred for 4hrs. The particles were separated by ultracentrifugation and washed with water. The final product was dried, ground and annealed at 500 °C for 4 h to remove volatile impurities indicates in Fig.1.

2.3. Characterization

The prepared nanocomposites were characterized by various instrumental techniques. UV-Vis spectra of the samples were taken using JASCO-V 530 dual beam spectrophotometer in the wavelength region 200 to 900 nm with a scanning speed of 400 nm/min. The FT-IR measurements of prepared nanocomposites as KBr disks were performed on a Thermo Scientific Nicolet iS5 FT-IR spectrometer in the frequency range of 400 to 4000 cm^{-1}. The morphological studies of the nanocomposites were carried out using Field Emission Scanning Electron Microscope (FESEM) with Energy Dispersive X-ray Spectroscopy (EDS) using TESCAN MIRA3 XMU. The SEM/EDS measurements were performed with the working distance of 6.5 mm, acceleration voltage is 10 kV and the aperture of 30 µm. Electrochemical workstation CHI 650C (CH Instruments, USA) was employed for electrochemical and electro analytical studies. This instrument uses the latest analogy and microcomputer design to provide high performance, better precision and greater versatility in electrochemical measurements and impedance studies.

3. RESULTS AND DISCUSSION

3.1. Band gap energy

The optical properties of (Ce/Mo/V) mixed metal oxide nanoparticles were studied by UV-visible absorption spectroscopy in the range of 200−900 nm and are shown in Fig 2. UV-Vis studies show absorption at 237 nm due to π-π* transition[35]. A broad band absorption at 308 nm, which might be because of the charge transfer between vanadium VO_4^{3-} in $CeVO_4$ (cerium orthovanadate) and oxygen [36]. The absorbance usually depends on numerous factors such as lattice strain, surface roughness, oxygen deficiency, impurity centres, band gap, and grain size.The band gap energy was calculated by using the Tauc's equation,

$$\alpha h\nu = B\left(h\nu - E_g\right)^m \quad \text{----------(1)}$$

Where, (α) = molar absorptivity, Planks constant (h) = 6.626×10^{-34}Joules sec, Frequency of Light (ν), m is the value of electronic transition type which is equal to 2 for direct transitions or ½ for indirect transitions of the materials respectively. The plot is drawn between $(\alpha h\nu)^{1/2}$ on y-axis and hν on y-axis respectively for the calculation of band gap energy (eV) of the material. From the graph there is a curve obtained which is extrapolated from straight path in the direction of its energy axis and gets the band gap energy valueto be 4.2 eV from Fig 2(a)

ISSN: 2515-8260, Volume 07, Issue 11, 2020

through equation (1). The highest band gap energy value broadens the valance and conduction bands space and make available support to keep away from reunion of hole pairs and electrons. This aspect perhaps complimentary for the oxidation and reduction reactions takes place in its surface and also due to the quantum confinement effect.

3.2. Functional analysis

FT-IR spectra serves as a powerful tool for identifying the functional groups. FTIR spectra of (Ce/Mo/V)MMO were recorded in the range of 400−4000 $cm^{-1}$and shown in Fig.3. The broad peak absorption around 3170 cm^{-1}, 1638 cm^{-1} and 1400 cm^{-1}can be assigned to stretching and bending vibrational frequencies of the OH groups of adsorbed H_20 molecule on the surface of the nanocomposites [37,38]. The band at 805 cm^{-1} is attributed to stretching vibrational mode of Mo-OH bond Mo-O bonds (Mo^{5+}, Mo^{6+} or Mo^{4+}) [39][36].The band at 718 cm^{-1} corresponds to Mo-OH double bond [40]. The V–O stretching vibration is seen at 616cm^{-1}[41] and Ce–O stretching is seen at 469cm^{-1}[42].

3.3. X-ray Diffraction analysis

Fig 4. Shows the XRD patterns for (Ce/Mo/V)MMO, the diffraction peaks at 2θ values at 19^0, 25^0, 29^0, 31^0, 34^0, 39^0, 48^0, 49^0, 53^0, 58^0, 59^0 and 75^0 are related to (010), (210), (111), (300), (220), (410), (320), (021), (311), (334), (222) and (331). Furthermore, the reflections at 29^0, 53^0, 59^0 and 75^0 are matches with the JCPDS card no- 34-0394 [43] for CeO_2. The peak at 25^0, 31^0, 34^0 and 58^0 are matching with the JCPDS card no- 21-0569 [44,45] for MoO_3. The peak positions 19^0, 39^0, 48^0 and 49^0 are matches with the JCPDS card no- 89-0612 [46] for V_2O_5.

The crystallite size of the sample is calculated using Scherrer formula [47]

$$D = \frac{N\lambda}{\beta \cos\theta} \text{ ---------- (2)}$$

Where 0.9 is the shape factor of the crystallites, d = average particle size, β is (FWHM), θ is the Bragg angle, λ is the wavelength of Cu Ka in radians. The crystallite size of the synthesized nanocomposites is calculated as 44.66 nm using equation (2).

3.4. Morphology of the (Ce/Mo/V)MMO

The surface morphology and microstructures of as-prepared nanocomposites was characterized using a scanning electron microscope. Fig 5(a) Shows particles of different sizes and shapes within the nanometer range. The aggregation may be due to drying. It shows a regular flake like structure. This is may be due to a regular arrangement of nanocomposites in the presence of surfactant. Fig 5(b) Shows EDS analysis of (Ce/Mo/V) mixed metal oxide nanocomposites. The spectrum indicates that a synthesized mixed metal oxide nanocomposite contains cerium, vanadium and molybdenum in the form of oxide in agreement with the chemical composition of the nanocomposite[48].

4. ELECTROCHEMICAL STUDIES FOR CAPACITOR APPLICATION

The working electrode was prepared by a slurry approach where 80 % wt. of the synthesized nanocomposite were combined with 15 % of conductive carbon and 5 % wt. of Poly tetra fluoroethylene (PTFE) in 1-methyl-2-pyrrolidinone (NMP). The slurry was spread over a grafoil sheet of (1x 1) cm^2 and it was dried in a hot air oven at a temperature of 60^OC for 12 h. Electrochemical performances were taken using three electrodes set up with 1 M KOH electrolyte and the tested samples were coated grafoil sheet as working electrodes. Platinum

wire and Ag/AgCl electrodes were used as counter and reference electrodes respectively.

4.1. Cyclic voltammetric studies

The specific capacitance of the nanocomposites is evaluated by cyclic voltammetric (CV) technique by recording the potential-current changes at different scan rates 5, 10, 20, 30, 50 and 100 in the potential ranging from 0 to +0.5 V. The voltammogram recorded is shown in Fig 6. Once the value of the scan rate increases from 5 mV/s to 100 mV/s, the loop of the CV also increases. This is because of the current increases as well as the voltage increases. The shape of the CV curves representing rigorous polarization and slower charge transfer in the metal oxide nanocomposite. When the scan rate was increased from 5 to 100 mV / s, the electrode current was increasing progressively from 0 V-+0.5 V in the anode scanning process and the cathode scanning process, without apparent redox peaks. In this process, the reaction take place between solution and electrode, adsorption and desorption occur.

The specific capacitance (Cp) was calculated by using the formula,

$$C_P = A / 2mk\Delta V \text{ ------- (3)}$$

Where, C_p is in F/g. A is the area inside cyclic voltammogram having units AV, m is the mass of active material, k is the scan rate of CV in volts per second and ΔV is the voltage range,
The value of capacitance decreased as the pH of the solution increased [49]. From table.1, the specific capacitance value is maximum for lower scanrates and it is decreased when the scanrates increases. The specific capacitance for 5mV/s(102 F/g) is higher than 100 mV/s scan rate using equation (3). The unique features of supercapacitors, like high capacitance and from the plot of specific capacitance Vs scan rate Fig.7, the capacitance value decreased at higher scan rates, which is the reason for high stability of the capacitance material and ion diffusion limitations [50].

4.2. Electrochemical impedance study (EIS)

The Nyquist plots of synthesized nanocomposite is shown in Fig.8, and it is clear that the peak of the semicircles appears at the low-frequency region. Generally, a semicircle in the medium-frequency region is related to the charge transfer process, and an inclined line in the low-frequency region symbolizes the Warburg impedance. Double-layer capacitance values (C_{dl}) and charge-transfer resistance values (R_{ct}) were obtained from impedance measurements. For Nyquist plots, it is clear that the impedance diagrams contain semicircles with the centre under the real axis. The size of the semicircle increases with the inhibitor concentration, indicating the charge transfer process, and the diameter of the semicircle is, therefore, equal to the polarization resistance.

According to the curve of Z' and Z'' values for mixed metal oxide, this results in the shrinking of the impedance plot, which is apparent from Fig.8. The Simplified Randel's cell is one of the most common cell models (Fig.9); it includes a solution resistance (Rs), a double-layer capacitor, and a charge transfer (R_{ct}) (or) polarization resistance (R_p). The double-layer capacitance is in parallel with the charge transfer resistance and its values are tabulated in table.2. This resistance reveals that at the electrode interface, there is redox behaviour of electron transfer dynamics.EIS spectrum indicates more straight line due to diffusion resistance. The higher surface area increases the interaction electrode surface and MMO which facilitates its better capacitive behaviour of the active electrode material [51].

5. CONCLUSION

The mixed metal oxide nanocomposite of(Ce/Mo/V) was synthesized and they were analysed by UV-Vis, FT-IR, FE-SEM, EDS, Cyclic voltammetry and EIS. FT-IR spectral analysis confirmed the functional group interactions with V–O, Mo-O and Ce–O stretching vibration.

ISSN: 2515-8260, Volume 07, Issue 11, 2020

Both XRD and EDS results reveals thepresence of mixed metal oxides, crystallinity and morphology of nanocomposites. The surface morphology of FE-SEM images shows that the surfaces with highly agglomerated grains and also the nanocomposite is in the nanometre range. From Cyclic voltammetric studies the specific capacitance value is 102 F/g which indicates the good performance for supercapacitor. Due to the higher specific capacitance value (102 F/g) of the MMO and can be utilized for supercapacitor electrode material in batteries and for future nano electronic devices. An EIS study of the nanocomposite provides electrode and electrolyte charge transfer behaviour and gives the capacitance value ($1.265x10^{-6}$ μFcm^{-2}). Such nanocomposite can be used in many fields such as sensors, solar cells and also as catalysts.

6. ACKNOWLEDGEMENT

The authors are thankful to PG and Research Department of chemistry, V. O. Chidambaram College, Thoothukudi-8 and Tamilnadu Adithravidar welfare department, Chepauk, Chennai-600005.

Fig 1. Preparation method of (Ce/Mo/V)MMO
Fig 2.UV-Vis spectrum and Tauc plot of (Ce/Mo/V)MMO.
Fig 3. FTIR image of (Ce/Mo/V)MMO with stretching vibration.
Fig 4.XRD pattern of (Ce/Mo/V)MMO with the corresponding peaks.
Fig 5.a) FE-SEM-image of mixed metal oxide corroborates the nano size and the presence of nanocomposites. (b) The chemical compositions of (Ce/Mo/V)MMOwith the respective EDS spectra.
Fig 6. Cyclic voltammogramof (Ce/Mo/V)MMO forvariousscanrates.
Fig 7. Plot of Specific capacitance Vs Scan rate of 5-100 mV/s.
Fig 8. Nyquist plot of (Ce/Mo/V)MMO.
Fig 9. Simplified Randles cell schematic diagram with the solution resistance (Rs), a double-layer capacitor, a charge transfer (Rct) and polarization resistance (Rp).
Table 1. Calculated values of specific capacitance of (Ce/Mo/V)MMO nanocomposites.
Table 2. R_s, R_{ct} and C_{dl} values of (Ce/Mo/V)MMO nanocomposites from EIS.

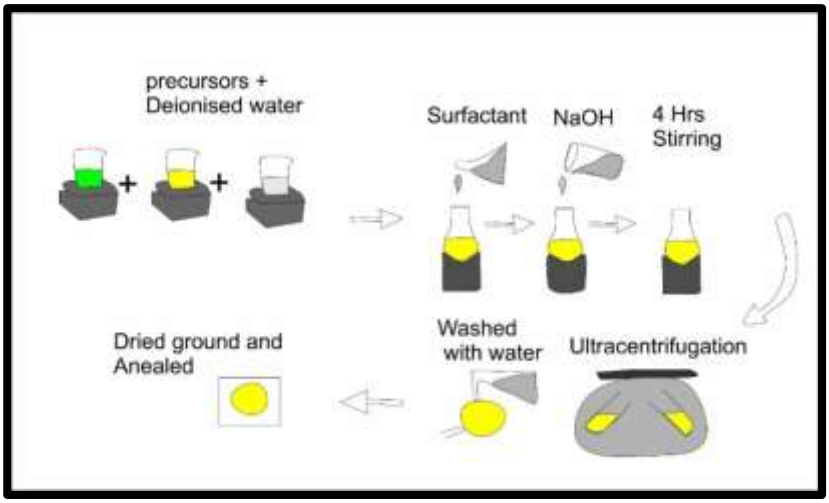

Fig 1. Preparation method of (Ce/Mo/V)MMO

ISSN: 2515-8260, Volume 07, Issue 11, 2020

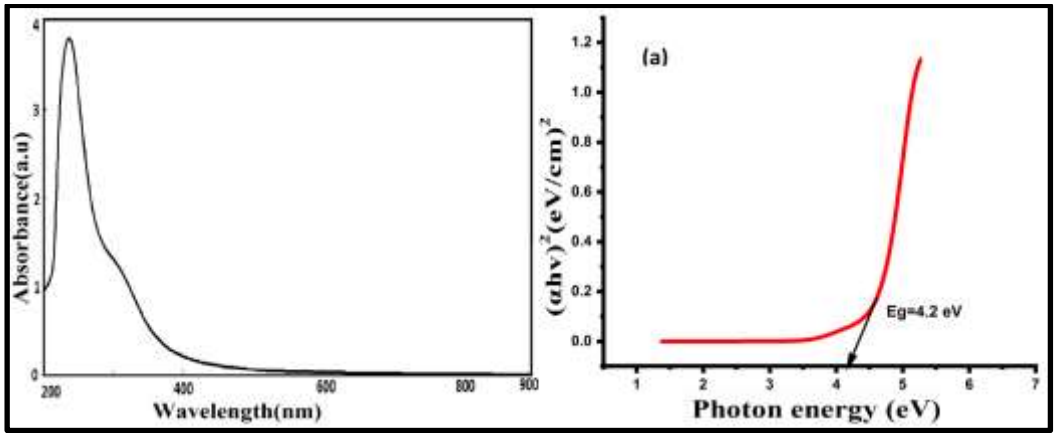

Fig 2. UV-Vis spectrum and Tauc plot of (Ce/Mo/V)MMO

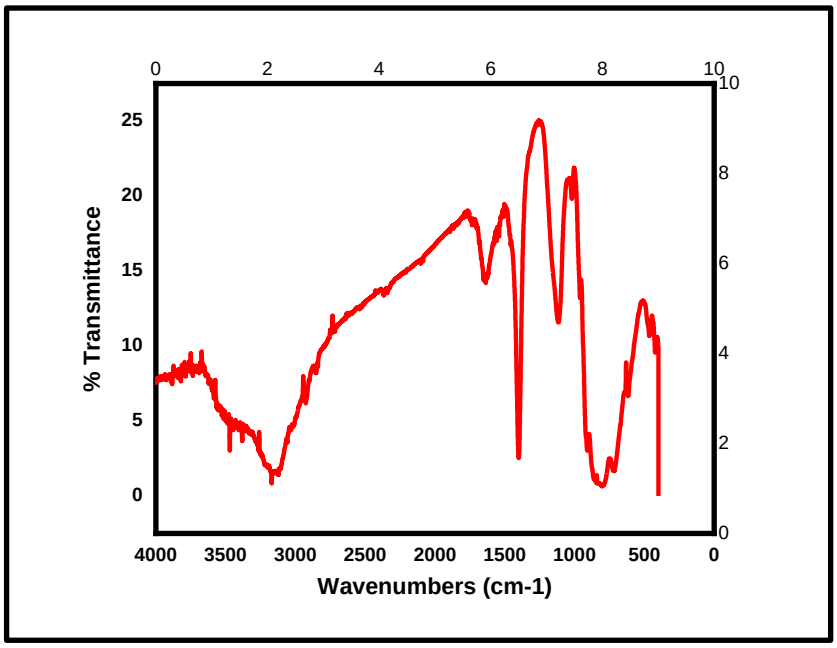

Fig 3. FTIR image of (Ce/Mo/V)MMO

ISSN: 2515-8260, Volume 07, Issue 11, 2020

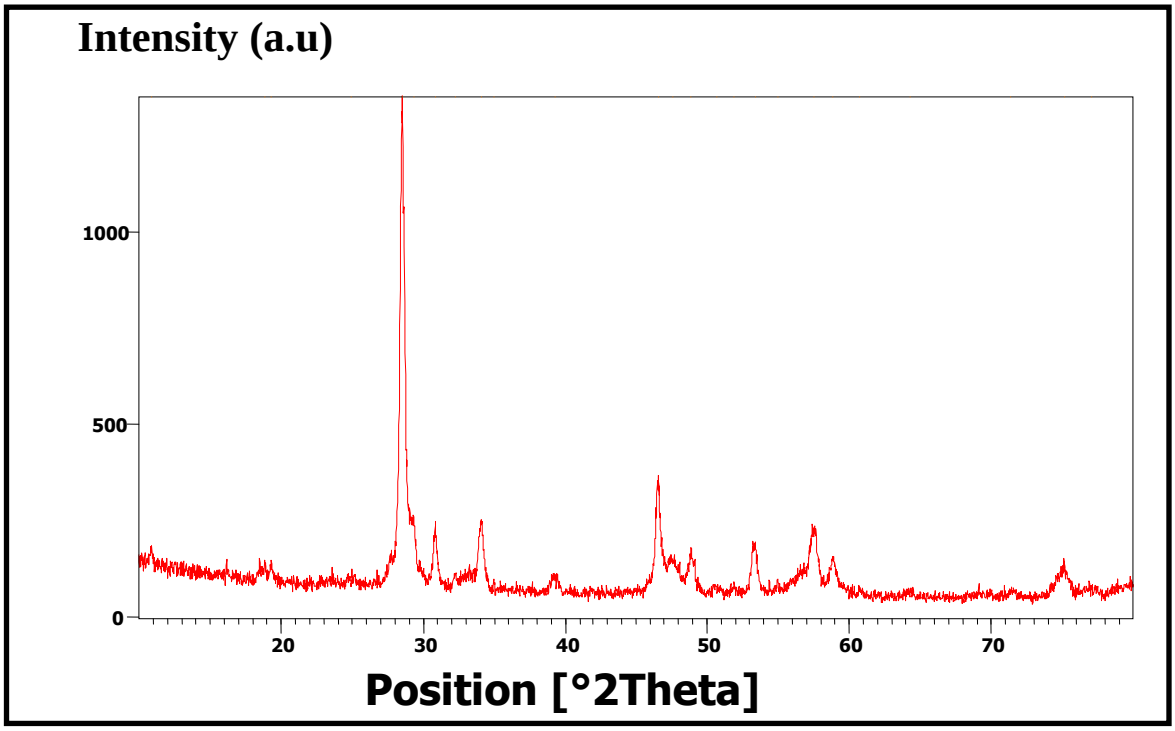

Fig 4.XRD pattern of (Ce/Mo/V)MMO

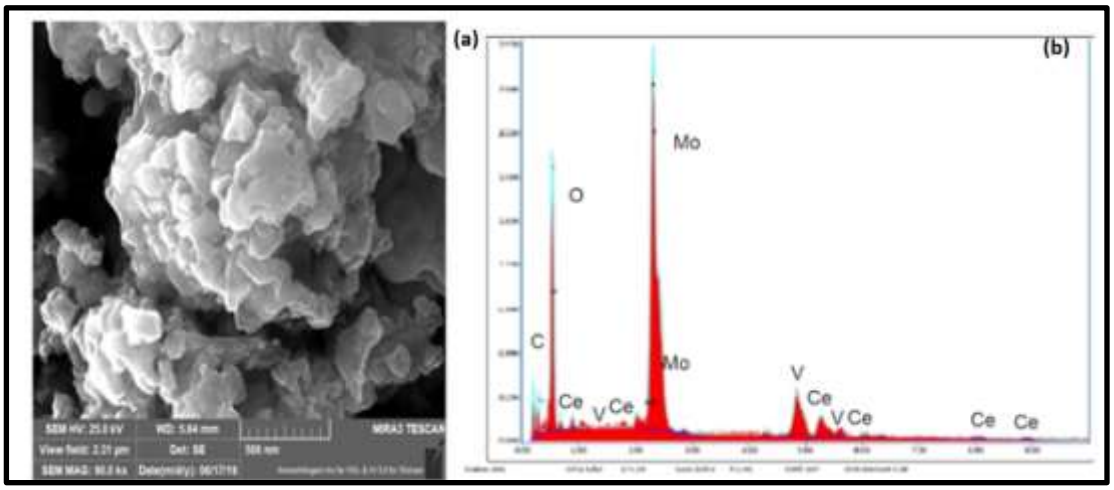

Fig 5 (a) FESEM (b) EDS of (Ce/Mo/V)MMO

ISSN: 2515-8260, Volume 07, Issue 11, 2020

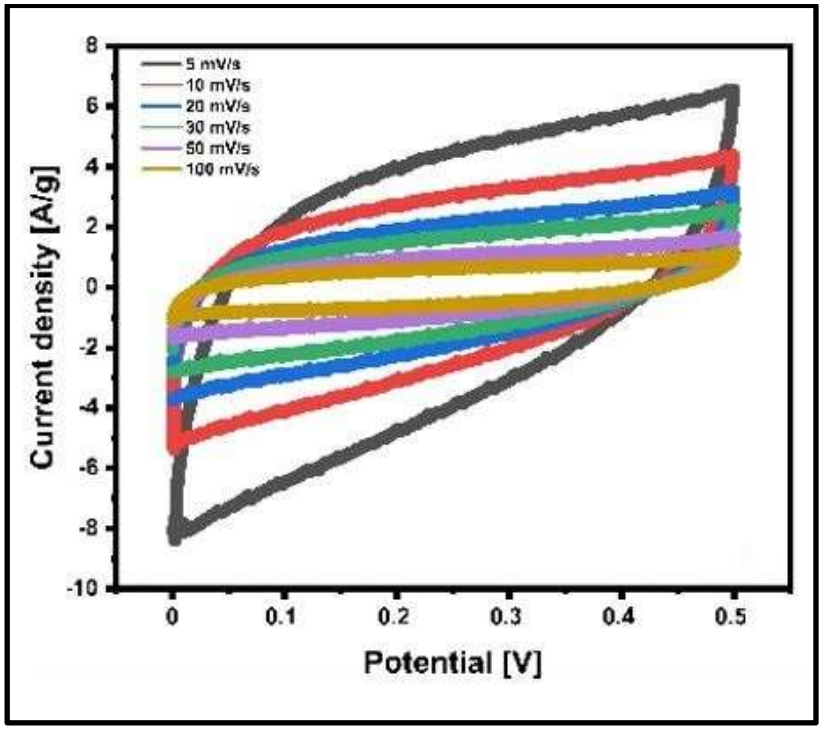

Fig 6. Cyclic voltammogramof (Ce/Mo/V)MMO

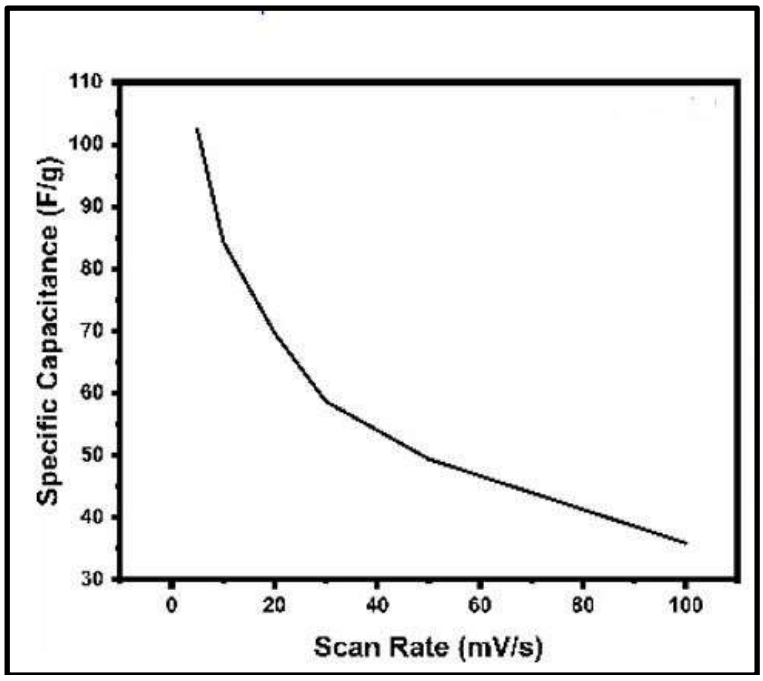

Fig 7. Plot of Specific capacitance Vs Scan rate

ISSN: 2515-8260, Volume 07, Issue 11, 2020

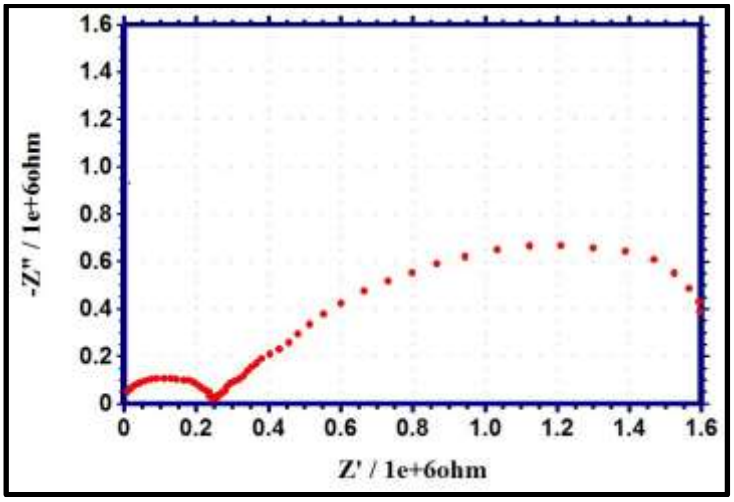

Fig 8. Nyquist plot of (Ce/Mo/V)MMO

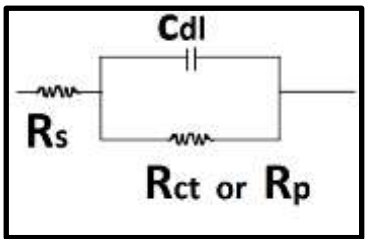

Fig 9. Simplified Randel's Cell Schematic Diagram

Table 1. Calculated values of specific capacitance of (Ce/Mo/V)MMO nanocomposites

Composite	Scanrate (k) (mVs^{-1})	C_p(F/g)
(Ce/Mo/V)MMO	5	102
	10	84
	20	70
	30	59
	50	49
	100	36

Table 2. R_s, R_{ct} and C_{dl} values of (Ce/Mo/V)MMO nanocomposites from EIS

Composite	SolutionResistanceR_S(Ohm)	Charge Transfer Resistance Rct(Ωcm^2)	Double layer capacitance Cdl(μFcm^{-2})
(Ce/Mo/V)MMO	$1.058x10^4$	$1.069x10^6$	$1.265x10^{-6}$

ISSN: 2515-8260, Volume 07, Issue 11, 2020

7. REFERENCE

[1] P. Simon, Y. Gogotsi, Materials for electrochemical capacitors, Nature materials, 7 (2008) 845-854.
[2] A. Balducci, R. Dugas, P.-L. Taberna, P. Simon, D. Plee, M. Mastragostino, S. Passerini, High temperature carbon–carbon supercapacitor using ionic liquid as electrolyte, Journal of power sources, 165 (2007) 922-927.
[3] H.-K. Jeong, M. Jin, E.J. Ra, K.Y. Sheem, G.H. Han, S. Arepalli, Y.H. Lee, Enhanced electric double layer capacitance of graphite oxide intercalated by poly (sodium 4-styrensulfonate) with high cycle stability, Acs Nano, 4 (2010) 1162-1166.
[4] J.R. Miller, P. Simon, Electrochemical capacitors for energy management, science, 321 (2008) 651-652.
[5] G. Wang, L. Zhang, J. Zhang, A review of electrode materials for electrochemical supercapacitors, Chemical Society Reviews, 41 (2012) 797-828.
[6] H. Gao, F. Xiao, C.B. Ching, H. Duan, High-performance asymmetric supercapacitor based on graphene hydrogel and nanostructured MnO_2, ACS applied materials & interfaces, 4 (2012) 2801-2810.
[7] M. Winter, R.J. Brodd, What are batteries, fuel cells, and supercapacitors?, Chemical reviews, 104 (2004) 4245-4270.
[8] C. Liu, Z. Yu, D. Neff, A. Zhamu, B.Z. Jang, Graphene-based supercapacitor with an ultrahigh energy density, Nano letters, 10 (2010) 4863-4868.
[9] X. Wang, Y. Zhang, J. Zheng, H. Jiang, X. Dong, X. Liu, C. Meng, Fabrication of vanadium sulfide (VS_4) wrapped with carbonaceous materials as an enhanced electrode for symmetric supercapacitors, Journal of colloid and interface science, 574 (2020) 312-323.
[10] Ramirez-Castro, C., Schütter, C., Passerini, S., & Balducci, A. (2016). Microporous carbonaceous materials prepared from biowaste for supercapacitor application. Electrochimica Acta, 206, 452-457.
[11] Chen, M., Zhang, Y., Liu, Y., Wang, Q., Zheng, J., & Meng, C. (2018). Three-dimensional network of vanadium oxyhydroxide nanowires hybridize with carbonaceous materials with enhanced electrochemical performance for supercapacitor. ACS Applied Energy Materials, 1(10), 5527-5538.
[12] Meng, Q., Cai, K., Chen, Y., & Chen, L. (2017). Research progress on conducting polymer based supercapacitor electrode materials. Nano Energy, 36, 268-285.
[13] Shown, I., Ganguly, A., Chen, L. C., & Chen, K. H. (2015). Conducting polymer-based flexible supercapacitor. Energy Science & Engineering, 3(1), 2-26.
[14] J. Fernando, C. Vedhi, Synthesis, spectral and electrochemical characterization of adipic acid doped polyaniline, The International Journal of Science and Technoledge, 3 (2015) 166.
[15] P. Manisankar, C. Vedhi, G. Selvanathan, R. Somasundaram, Electrochemical and electrochromic behavior of novel poly (aniline-co-4, 4 '-diaminodiphenyl Sulfone), Chemistry of materials, 17 (2005) 1722-1727.
[16] Abdah, M. A. A. M., Azman, N. H. N., Kulandaivalu, S., & Sulaiman, Y. (2020). Review of the use of transition-metal-oxide and conducting polymer-based fibres for high-performance supercapacitors. Materials & Design, 186, 108199.
[17] Low, W. H., Khiew, P. S., Lim, S. S., Siong, C. W., & Ezeigwe, E. R. (2019). Recent development of mixed transition metal oxide and graphene/mixed transition metal oxide based hybrid nanostructures for advanced supercapacitors. Journal of Alloys and Compounds, 775, 1324-1356.
[18] Ahuja, P., Ujjain, S. K., & Kanojia, R. (2018). Electrochemical behaviour of manganese & ruthenium mixed oxide@ reduced graphene oxide nanoribbon composite in symmetric and asymmetric supercapacitor. Applied Surface Science, 427, 102-111.

[19] Kulandaivalu, S., & Sulaiman, Y. (2019). Designing an advanced electrode of mixed carbon materials layered on polypyrrole/reduced graphene oxide for high specific energy supercapacitor. Journal of Power Sources, 419, 181-191.
[20] Peng, R., Zhang, H., Gui, L., Zheng, Y., Wu, Z., Luo, Y., & Yu, P. (2019). Construction of 0D CeO_2/2D MnO_2 heterostructure with high electrochemical performance. Electrochimica Acta, 319, 95-100.
[21] Jiang, Q., Kurra, N., Alhabeb, M., Gogotsi, Y., & Alshareef, H. N. (2018). All pseudocapacitive MXene-RuO_2 asymmetric supercapacitors. Advanced Energy Materials, 8(13), 1703043.
[22] Li, P., Chen, X., Li, Y., & Schwank, J. W. (2019). A review on oxygen storage capacity of CeO_2-based materials: Influence factors, measurement techniques, and applications in reactions related to catalytic automotive emissions control. Catalysis today, 327, 90-115.
[23] Z. Zhai, D. Cui, Y. Zhang, Y. Hou, M. Cui, H. Zhang, J. Song, H. Wang, Effects of loading transition metal (Mn, Cr, Fe, Cu) oxides on oxygen storage/release properties of CeO_2-ZrO_2 solid solution, Journal of Rare Earths, 38 (2020) 274-280.
[24] Parthiban, K., Pazhanivel, K., & Muthiya, S. J. (2017). Emission control in multi-cylinder spark ignition engines using metal-oxide coated catalytic converter. International Journal of Vehicle Structures & Systems, 9(2), 134.
[25] Dey, S., & Dhal, G. C. (2020). Controlling carbon monoxide emissions from automobile vehicle exhaust using copper oxide catalysts in a catalytic converter. Materials Today Chemistry, 17, 100282.
[26] Tripathy, N., & Kim, D. H. (2018). Metal oxide modified ZnO nanomaterials for biosensor applications. Nano convergence, 5, 1-10.
[27] George, J. M., Antony, A., & Mathew, B. (2018). Metal oxide nanoparticles in electrochemical sensing and biosensing: a review. Microchimica Acta, 185, 1-26.
[28]Karthikeyan, C., Jenita Rani, G., Ng, F. L., Periasamy, V., Pappathi, M., Jothi Rajan, M., ... & Gnana kumar, G. (2020). 3D Flower–Like $FeWO_4$/CeO_2 Hierarchical Architectures on rGO for Durable and High-Performance Microalgae Biophotovoltaic Fuel Cells. Applied biochemistry and biotechnology, 192, 751-769.
[29] Hu, S., Li, W., Finklea, H., & Liu, X. (2020). A review of electrophoretic deposition of metal oxides and its application in solid oxide fuel cells. Advances in colloid and interface science, 276, 102102.
[30] A. Yari, S. Heidari Fathabad, A high-performance supercapacitor based on cerium molybdate nanoparticles anchored on N, P co-doped reduced graphene oxide nanocomposite as the electrode, Journal of Materials Science: Materials in Electronics, 31 (2020) 13051-13062.
[31] S.C. Sekhar, G. Nagaraju, B. Ramulu, J.S. Yu, Hierarchically designed Ag@ $Ce_6Mo_{10}O_{39}$ marigold flower-like architectures: an efficient electrode material for hybrid supercapacitors, ACS applied materials & interfaces, 10 (2018) 36976-36987.
[32] N. Padmanathan, S. Selladurai, Shape controlled synthesis of CeO_2 nanostructures for high performance supercapacitor electrodes, RSC advances, 4 (2014) 6527-6534.
[33] P. Gao, R.J. Koch, A.C. Ladonis, S.T. Misture, One-Step Solvothermal Preparation of Mn-Doped VO_2 (B) Nanosheets for High-Performance Supercapacitors, Journal of The Electrochemical Society, 167 (2020) 160523.
[34] Naderi, H. R., Ghaderi, A., Seyedi, Z. S., & Eghbali-Arani, M. (2019). Facile synthesis and characterization of $CeMoO_4$ nanostructure via co-precipitation method and investigate its application supercapacitor. Analytical and Bioanalytical Electrochemistry, 11(6), 679-690.
[35]. Ebrahimi, I., & Parvinzadeh Gashti, M. (2015). Extraction of juglone from Pterocarya fraxinifolia leaves for dyeing, anti-fungal finishing, and solar UV protection of wool. Coloration Technology, 131(6), 451-457.

[36] Liu, Q. Q., Fan, C. Y., Tang, H., Ma, T. D., & Shen, J. Y. (2016). One-step synthesis of recycled 3D $CeVO_4$/rGO composite aerogels for efficient degradation of organic dyes. RSC advances, 6(89), 85779-85786.
[37] Sagadevan, S., Venilla, S., Marlinda, A. R., Johan, M., Wahab, Y. A., Zakaria, R., ... & Ahmad, N. (2020). Effect of synthesis temperature on the morphologies, optical and electrical properties of MgO nanostructures. Journal of nanoscience and nanotechnology, 20(4), 2488-2494.
[38] Song, J., Ni, X., Gao, L., & Zheng, H. (2007). Synthesis of metastable h-MoO_3 by simple chemical precipitation. Materials Chemistry and Physics, 102(2-3), 245-248.
[39] Maheswari, N., & Muralidharan, G. (2017). Controlled synthesis of nanostructured molybdenum oxide electrodes for high performance supercapacitor devices. Applied surface science, 416, 461-469.
[40] Hu, H., Deng, C., Xu, J., Zhang, K., & Sun, M. (2015). Metastable h-MoO_3 and stable α-MoO_3 microstructures: controllable synthesis, growth mechanism and their enhanced photocatalytic activity. Journal of Experimental Nanoscience, 10(17), 1336-1346.
[41] Andronache, C. I., & Racolta, D. (2014, November). Structural investigation of $MO\cdot P_2O_5\cdot Li_2O$ (MO= Fe_2O_3 or V_2O_5) glass systems by FTIR spectroscopy. In AIP Conference Proceedings (Vol. 1634, No. 1, pp. 115-119). American Institute of Physics.
[42] Syed, A., Yadav, L. S. R., Bahkali, A. H., Elgorban, A. M., Abdul Hakeem, D., & Ganganagappa, N. (2020). Effect of CeO_2-ZnO Nanocomposite for Photocatalytic and Antibacterial Activities. Crystals, 10(9), 817.
[43] Yuan, S., Zhang, Q., Xu, B., Jin, Z., Zhang, Y., Yang, Y., ... & Ohno, T. (2014). Porous cerium dioxide hollow spheres and their photocatalytic performance. RSC advances, 4(107), 62255-62261.
[44] Chithambararaj, A., & Bose, A. C. (2014). Role of synthesis variables on controlled nucleation and growth of hexagonal molybdenum oxide nanocrystals: investigation on thermal and optical properties. CrystEngComm, 16(27), 6175-6186.
[45] Liu, Y., Feng, P., Wang, Z., Jiao, X., & Akhtar, F. (2017). Novel fabrication and enhanced photocatalytic MB degradation of hierarchical porous monoliths of MoO_3 nanoplates. Scientific Reports, 7(1), 1845.
[46] Butt, F. K., Cao, C., Idrees, F., Tahir, M., Hussain, R., & Alshemary, A. Z. (2015). Fabrication of V_2O_5 super long nanobelts: optical, in situ electrical and field emission properties. New Journal of Chemistry, 39(7), 5197-5202.
[47] Vorokh, A. S. (2018). Scherrer formula: estimation of error in determining small nanoparticle size. Наносистемы: физика, химия, математика, 9(3), 364-369.
[48]Hou, S. X., Wu, C., & Huo, Y. J. (2017). Controllable preparation of nano molybdenum disulfide by hydrothermal method. Ceramics–Silikáty, 61(2), 158-162.
[49] M. Naumowicz, Z.A. Figaszewski, The Effect of pH on the Electrical Capacitance of Phosphatidylcholine–Phosphatidylserine System in Bilayer Lipid Membrane, The Journal of membrane biology, 247 (2014) 361-369.
[50] Roberts, M. E., Wheeler, D. R., McKenzie, B. B., & Bunker, B. C. (2009). High specific capacitance conducting polymer supercapacitor electrodes based on poly (tris (thiophenylphenyl) amine). Journal of Materials Chemistry, 19(38), 6977-6979.
[51]Sharon, D., Bennington, P., Liu, C., Kambe, Y., Dong, B. X., Burnett, V. F., ... & Nealey, P. F. (2018). Interrogation of electrochemical properties of polymer electrolyte thin films with interdigitated electrodes. Journal of The Electrochemical Society, 165(16), H1028.